PAPER • OPEN ACCESS

Contribution of Jahn-Teller and charge transfer excitations to the photovoltaic effect of manganite/titanite heterojunctions

To cite this article: Benedikt Ifland *et al* 2017 *New J. Phys.* **19** 063046

New Journal of Physics
The open access journal at the forefront of physics

Deutsche Physikalische Gesellschaft DPG
IOP Institute of Physics

Published in partnership with: Deutsche Physikalische Gesellschaft and the Institute of Physics

OPEN ACCESS

RECEIVED
22 December 2016

REVISED
21 March 2017

ACCEPTED FOR PUBLICATION
7 April 2017

PUBLISHED
30 June 2017

PAPER

Contribution of Jahn-Teller and charge transfer excitations to the photovoltaic effect of manganite/titanite heterojunctions

Benedikt Ifland[1], **Joerg Hoffmann**[1], **Birte Kressdorf**[1], **Vladimir Roddatis**[1], **Michael Seibt**[2] and **Christian Jooss**[1,3,4]

[1] University of Goettingen, Institute of Materials Physics, Friedrich-Hund-Platz 1, 37077 Goettingen, Germany
[2] University of Goettingen, 4th Physical Institute, Friedrich-Hund-Platz 1, 37077 Goettingen, Germany
[3] International Center for Advanced Studies of Energy Conversion (ICASEC), Georg-August-University, D-37077 Göttingen, Germany
[4] Author to whom any correspondence should be addressed.

E-mail: jooss@material.physik.uni-goettingen.de

Keywords: perovskite oxide, photovoltaic effect, strong correlations

Supplementary material for this article is available online

Abstract

The effect of correlation effects on photovoltaic energy conversion at manganite/titanite heterojunctions is investigated. As a model system we choose a heterostructure consisting of the small polaron absorber $Pr_{0.66}Ca_{0.34}MnO_3$ (PCMO) epitaxially grown on single-crystalline Nb-doped $SrTi_{0.998}Nb_{0.002}O_3$ (STNO) substrates. The high structural and chemical quality of the interfaces is proved by detailed characterization using high-resolution transmission electron microscopy (TEM) and electron energy loss spectroscopy (EELS) studies. Spectrally resolved and temperature-dependent photovoltaic measurements show pronounced contributions of both the Jahn-Teller (JT) excitations and the charge transfer (CT) transitions to the photovoltaic effect at different photon energies. A linear temperature dependence of the open-circuit voltage for an excitation in the PCMO manganite is only observed below the charge-ordering temperature, indicating that the diffusion length of the photocarrier exceeds the size of the space charge region. The photovoltaic response is compared to that of a heterojunction of lightly doped $Pr_{0.05}Ca_{0.95}MnO_3$ (CMO)/STNO, where the JT transition is absent. Here, significant contributions of the CT transition to the photovoltaic effect set in below the Neel temperature. We conclude that polaronic correlations and ordering effects are essentials for photovoltaic energy conversion in manganites.

1. Introduction

Manganite perovskites with pronounced interactions between the spin, charge, orbital, and lattice degrees of freedom have attracted considerable interest because these correlations lead to a rich phase diagram [1, 2]. Dependent on temperature and carrier doping, various exotic phases emerge, including orbital [3], charge [4], and magnetically ordered ones [5]. The optical excitations of such phases include polaronic and charge transfer excitations [6–9], as well as cooperative excited states which may even lead to optically induced phase transitions at high photon fluences [10, 11]. Rectifying electrical behavior and photovoltaic responses to photon illumination have been widely demonstrated in manganite heterojunctions based on manganite films on n-type $SrTiO_3$ [12–16]. Such junctions thus offer opportunities to study new strategies for light harvesting, i.e. using polaronic excitations with long lifetimes [17, 18] or tuning the junction properties by external electric or magnetic fields [19, 20]. However, the understanding of the photovoltaic response of such heterojunctions is still very limited, since neither the involved optical transitions nor the mechanism of charge separation are clearly understood.

We have investigated manganite/titanite junctions, where epitaxial manganite films of two different doping levels ($Pr_{0.66}Ca_{0.34}MnO_3$ (PCMO) and $Pr_{0.05}Ca_{0.95}MnO_3$ (CMO)) have been prepared by ion beam sputter deposition on electron-doped $SrTi_{0.998}Nb_{0.002}O_3$ (STNO) single crystals. STNO can essentially be considered as

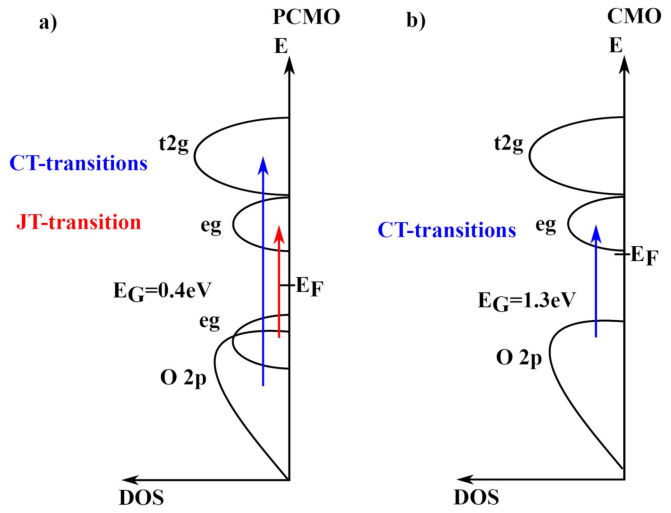

Figure 1. Schematic manganite density of states (DOS): (a) PCMO and (b) CMO.

a degenerated semiconductor with weak electron–phonon coupling giving rise to a 'metal-like' temperature dependence of resistivity. In contrast, the mobility in the manganite is governed by a thermally activated transport of small polarons [21, 22].

Since the band gap of the STNO is $E_{G,STNO} = 3.2$ eV, spectrally resolved measurements at photon energies below 3.2 eV allow for investigations of the manganite contribution to the photovoltaic effect of manganite/titanite heterojunctions (see also the spectrally resolved absorptance measurements; figure S1 is available at stacks.iop.org/NJP/19/063046/mmedia in supplemental material section A). In PCMO, the optical transition in the visible range up to 2 eV is governed by a dipole-allowed transition of polaronic nature from occupied lower Mn3d e_g states to antibonding σ type O2p-Mn3d e_g states that are split due to the Jahn-Teller (JT) effect [6, 23]. In the following, we name this transition a JT transition. For photon energies above 2.5 eV, charge transfer (CT) transitions from O2p to minority spin Mn3d t_{2g} and e_g states set in (see figure 1).

PCMO exhibits a first-order charge-ordering (CO) transition at about $T_{CO} \approx 240$ K and antiferromagnetic order below the Neel temperature $T_N \approx 160$ K. The CO transition in PCMO evolves via a two-phase regime of ordered and unordered domains over a broad temperature range [24–26], which is influenced by strain, twinning, and preparation-induced point defect disorder. As a consequence, the long-range polaron ordering in the CO phase can be considerably improved by additional post-growth annealing steps [27]. Based on temperature-dependent and spectrally resolved investigations of the photovoltaic parameters, i.e. the open-circuit voltage V_{OC} and the short-circuit current density J_{SC}, we conclude that both transitions contribute to the photovoltaic effect in the PCMO/STNO heterojunction. The results are compared to those of CMO/STNO junctions, where the JT splitting and the related 3d type polaronic excitations are entirely absent. Here, the optical excitations have a pure charge transfer character, presumably slightly modified by weak electron–phonon coupling. Furthermore, charge and orbital ordering is absent in CMO, but antiferromagnetic ordering below $T_N = 120$ K is present [28]. In those junctions, the contribution of manganite photoexcitations to the photovoltaic effect is strongly reduced.

2. Experimental details

PCMO and CMO thin films were prepared by ion beam sputtering of the respective targets in a high-vacuum chamber ($p_0 < 10^{-6}$ mbar). During deposition, the partial pressures were fixed to $p_{Ar} = 3 \cdot 10^{-4}$ mbar (beam neutralization), $p_{Xe} = 1 \cdot 10^{-4}$ mbar (sputtering) and $p_{O2} = 1.4 \cdot 10^{-4}$ mbar (film oxidation). For both types of samples, the deposition temperature was $T_{dep} = 750$ °C and the sputter power on the target was fixed to 4 W cm^{-2}.

Commercially available STNO substrates from Crystec served as a template for epitaxial growth and as the n-type part of the heterojunctions. Here we compare three different heterojunctions: A CMO/STNO junction and two PCMO/STNO junctions, as-prepared (a.p.) and after a post-growth annealing step in a furnace (p.a.) at 900 °C for 20 h in air. Such annealing steps cause partial annihilation of preparation-induced disorder defects, which significantly affect long-range ordering in PCMO. Since the alkaline earth-rich manganites are

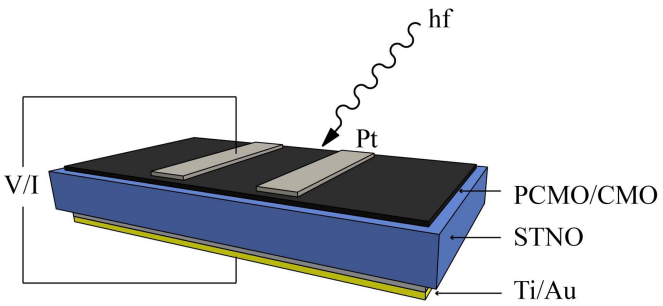

Figure 2. Sketch of the sample geometry for photovoltaic characterization. The (1×4 mm^2) Pt top contacts and the (4×9 mm^2) Ti/Au backside contact were prepared by using shadow masks. The illuminated area next to the top contact has a size of about 3×4 mm^2 (Xe-illumination) and 2×4 mm^2 (monochromator). All current densities mentioned in the text refer to the top electrode area. Illumination powers were fixed to 175 mW (Xe-illumination) and 200 μW (monochromator), respectively. The voltage polarity was set with respect to the top electrode, i.e. a positive current corresponds to a current from top to bottom.

thermodynamically less stable and tend to chemical phase decomposition, we have not performed additional post-growth annealing steps of the CMO-based junctions.

The crystal quality of the manganite layers was checked by x-ray diffraction (XRD) studies, which confirmed epitaxial growth without misorientations besides the commonly observed (001/220) twinning of PCMO films. Structural properties and the chemical composition of the near-interfacial regions were investigated by transmission electron microscopy (TEM) and electron energy loss spectroscopy (EELS). Both CMO/STNO and PCMO/STNO interfaces are almost dislocation free and the degree of intermixing is small (<2.5 nm). They mainly differ in the appearance of anti-phase boundaries (APBs) in the CMO, which extend toward the CMO/STNO interface and may represent recombination active defects. Further details of these investigations are shown in the supplemental material section B.

The sample geometry for electric characterization is shown in figure 2. The manganite layers with a thickness of about 75–100 nm were deposited at a temperature of $T_{dep} = 750$ °C. In order to avoid pronounced Schottky barriers, a Ti layer (200 nm) with a protective Au layer (100 nm) was previously deposited on the rear side of the STNO substrates. The deposition temperature was $T_{dep} = 200$ °C. Subsequently, Pt top layers (200 nm) were deposited at $T_{dep} = 200$ °C ensuring an ohmic electric contact to the manganite layers. The electric characterization was performed in a cryostat with a Suprasil entry window at temperatures between room temperature and 75 K. In order to measure the current–voltage dependence of the heterojunctions in the dark and under illumination, the top and rear side contacts were connected to a Keithley 2430, which served as voltage source and ammeter. The voltage drop between top and bottom electrodes was measured using a Keithley 2182A Nanovoltmeter with the convention of positive voltages corresponding to a positive top electrode potential.

Two different types of illumination were used: (1) Broad-band illumination (polychromatic) with a LOT (150 W) Xe-UV xenon lamp with Suprasil glass housing, and (2) spectrally resolved illumination with a 300 W Xe lamp equipped with a LOT Omni 300 monochromator The latter allows for an energy resolution of about 20 meV at a wavelength of about 500 nm. For the polychromatic illumination condition, a Laserpoint thermopile sensor was used to adjust the input power to 175 mW. In case of monochromatic illumination, the input power was adjusted to 200 μW using a calibrated Laserpoint Silicon diode. Note that the spectral fluxes of incident beams are comparable in order of magnitude, i.e. of the order of 29 mW eV^{-1} (polychromatic) and 10 mW eV^{-1} (monochromatic). In the following, all current densities are normalized to the small-sized top contact area (1×4 mm^2). The illuminated area beside the contact is about a factor of 2–3 larger than the top contact size.

3. Current–voltage (J–V) characteristics of manganite/titanite heterojunctions under polychromatic illumination

All junctions reveal rectifying behavior (see also figure S3 in supplemental material section C), i.e. an almost exponential increase of current in the forward direction and a small, only weakly voltage-dependent current in the reverse direction (negative voltages). Polychromatic illumination causes a clear photovoltaic effect (figure 3) appearing as pronounced open-circuit voltages $V_{OC}(J = 0)$ and short-circuit current densities $J_{SC}(V = 0)$. Figure 4(a) shows that the open-circuit voltage of the different junctions increases linearly with decreasing temperature with small deviations from the linear behavior occurring at rather low temperatures ($T < 150$ K). Interestingly, the slopes dV_{OC}/dT are very similar for all junctions but they differ in the intercept at T = 0. Post-

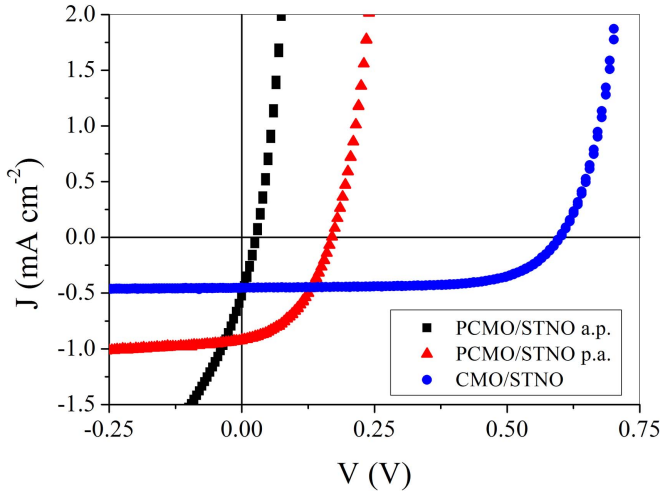

Figure 3. Current–voltage dependence of the different heterojunctions under Xe lamp illumination at 300 K. All junctions show a rectifying behavior and a photovoltaic effect in the analyzed temperature region.

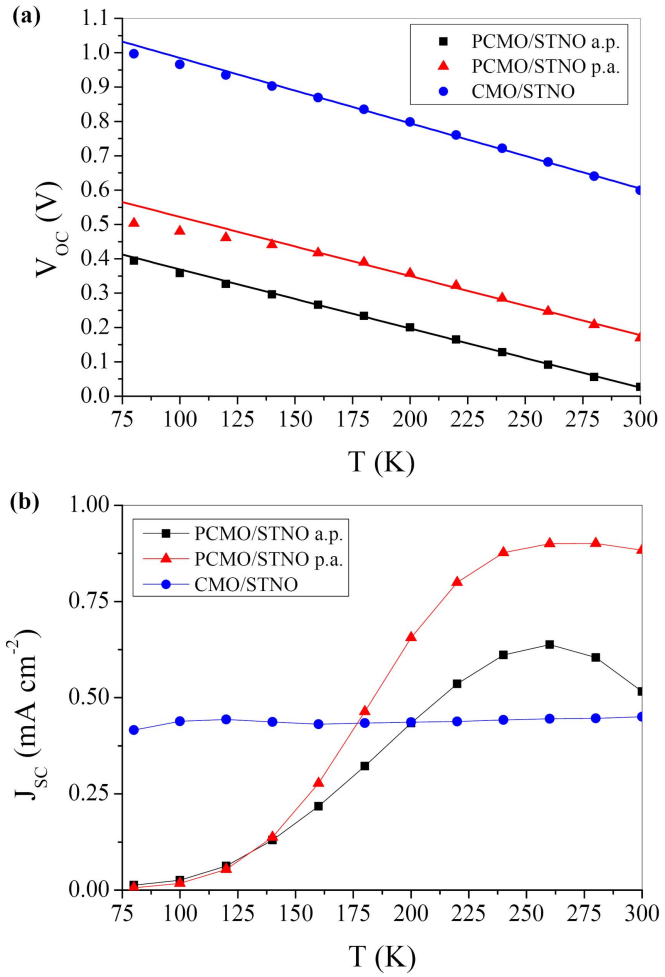

Figure 4. Temperature dependence of the characteristic photovoltaic properties: (a) the open-circuit voltage V_{OC} and (b) the short-circuit current density J_{SC} of the different heterojunctions under polychromatic illumination. The parameters were extracted from J–V curves under illumination with a Xe lamp at a constant temperature. In (a), the bold lines represent linear fits to the data. In (b), lines are guides for the eyes.

Table 1. Photovoltaic properties under polychromatic illumination. Slope and intercept of the linear part of the temperature-dependent open-circuit voltage V_{OC} and short-circuit current density J_{SC} near room temperature.

Heterojunction	dV_{OC}/dT (mV K^{-1})	$e \cdot V_{OC}(T \rightarrow 0)$ (meV)	J_{SC}(300 K) (μA cm^{-2})
PCMO/STNO (a.p.)	-1.72 ± 0.02	541 ± 4	$581 \pm 1 \cdot 10^{-3}$
PCMO/STNO (p.a.)	-1.72 ± 0.05	694 ± 11	872 ± 0.2
CMO/STNO	-1.90 ± 0.03	1175 ± 6	$438 \pm 8 \cdot 10^{-3}$

growth annealing of PCMO/STNO junctions is accompanied by a significant increase of the extrapolation $V_{OC}(T \rightarrow 0)$ from about 541(4) meV to 694(11) meV. For the CMO/STNO junction, the intercept amounts to 1175(6) meV.

The PCMO/STNO and CMO/STNO junctions exhibit pronounced differences in the temperature dependence of the short-circuit current densities (figure 4(b)). While CMO/STNO junctions reveal an almost temperature-independent J_{SC}, PCMO/STNO junctions show significantly higher short-circuit currents at high temperature, which steeply decrease with temperatures below 220 K, i.e. approximately below the charge-ordering temperature of PCMO films. Again, post-annealing is accompanied by improved photovoltaic properties, i.e. an increase of J_{SC} over the whole temperature range. The slope and intercept of the linear V_{OC} temperature dependence and short-circuit current density at room temperature are summarized in table 1.

4. Spectrally resolved photovoltaic characterization of manganite/titanite heterojunctions

In order to investigate the photovoltaic contributions of manganite and titanite transitions, spectrally resolved measurements of J–V characteristics were performed. We used different cut-off filters for studies with limited spectral ranges but with fixed illuminating power (figure 5). Reduction of the maximum photon excitation energy establishes the crossover from excitation in the manganite and the titanite to selective excitation of the manganite. This significantly affects the temperature dependence of the open-circuit voltage from linear to non-linear (figure 5(a)). However, the extrapolated zero-temperature values of V_{OC} are very similar. $V_{OC}(T \rightarrow 0)$ is thus rather independent of the spectral excitation range. Figure 5(b) shows the temperature dependence of the short-circuit current density J_{SC}. The current densities are normalized to J_{SC} under polychromatic illumination. Excluding excitations in STNO ($E_{ph} <= 2.8$ eV) current density yields about 20% of the full-xenon illumination current density at temperatures above 170 K and about 40% at low temperatures ($T = 70$ K). Successive reduction of the maximum excitation energies to the near-infrared range (NIR) drastically reduces the J_{SC}.

Figure 5(c) compares the temperature dependence of V_{OC} of the post-annealed PCMO/STNO junction under polychromatic and monochromatic illumination at $E_{ph} = 1.55$ eV. It is measured during continuous cooling under open-circuit conditions, i.e. by connecting the Keithley 2182A Nanovoltmeter with an internal resistance of >10 GΩ to the devices. Under polychromatic illumination the temperature dependence is linear and nicely matches V_{OC} deduced from J–V curves at fixed temperatures. Under monochromatic illumination, three different temperature regimes are observed in the $V_{OC}(T)$ curves. V_{OC} is very small near room temperature. It increases exponentially with decreasing temperature, i.e. $V_{OC} \propto \exp(E_B/kT)$ seems to be suppressed by a thermally activated process with an activation energy E_B. At lower temperatures, $V_{OC}(T)$ shows a nearly linear increase. It deviates from the linear increase at very low temperatures. The activation barrier E_B in the exponential regime as well as the slope dV_{OC}/dT and the intercept $V_{OC}(T \rightarrow 0)$ of the linear regime are summarized in table 2.

For the PCMO/STNO junctions, the crossover temperature from exponential to linear behavior of $V_{OC}(T)$ is at about $T_{CR} = 200$ K (figure 6(a)). Post-annealing does not strongly influence E_B in the exponential regime, but a broadening of the crossover region is visible in the calculated apparent activation energies (figure 6(b)). Remarkably, the activation barrier E_B and the intercept $V_{OC}(T \rightarrow 0)$ are nearly the same and are only slightly below the values of $V_{OC}(T \rightarrow 0)$ for polychromatic illumination.

CMO/STNO junctions under monochromatic illumination ($E_{ph} = 2.0$ eV) reveal a similar behavior, i.e. a crossover from exponential to linear temperature dependence (figure 6(c)) and an activation barrier E_B close to $V_{OC}(T \rightarrow 0)$ (table 2). However, the crossover temperature $T_{CR} = 125$ K is lower and close to the Neel temperature of CMO and $V_{OC}(T \rightarrow 0)$ is much smaller than when under polychromatic illumination.

The spectrally resolved contributions of manganite excitations, i.e. excitations with photon energies below the STNO band gap ($E_{G,STNO} = 3.2$ eV) are shown in figure 7. In a.p. PCMO/STNO junctions, the open-circuit voltage (figure 7(a)) and short-circuit current density (figure 7(b)) are almost constant in the spectral range from about 2.5 to 3 eV. Below 2.5 eV both quantities decrease, but a clear contribution remains from low-energy excitations down to 1.3 eV. The change in shape at about 1.8 eV indicates that two transitions are involved. Post-growth annealing does not change the overall dependence but significantly enhances V_{OC}, which is accompanied

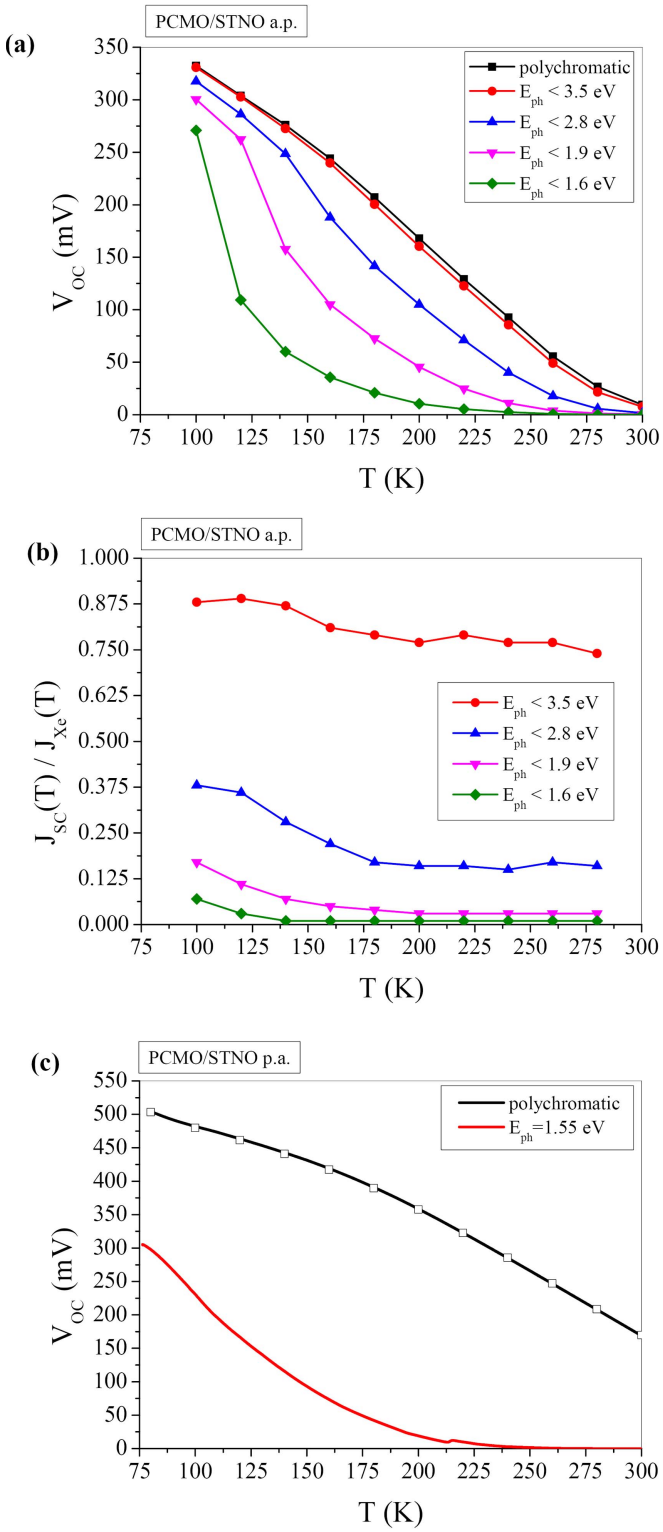

Figure 5. Temperature dependence of the spectral contributions to the open-circuit voltage V_{OC} and the short-circuit current density J_{SC} in PCMO/STNO junctions. J–V curves were measured after limiting the spectrum of the Xe lamp by different cut-off filters and keeping the illumination power constant. (a) Temperature dependence of V_{OC} for different cut-off filters of an a.p. sample. (b) Temperature dependence of J_{SC} normalized to the short-circuit current density $J_{SC,Xe}(T)$ under Xe lamp illumination for different cut-off filters of an a.p. sample. (c) Comparison of $V_{OC}(T)$ measured under Xe lamp illumination and monochromatic illumination with $E_{Ph} = 1.55$ during continuous cooling (solid lines) and deduced from J–V curves at constant temperatures (open symbols) of a post-annealed sample. The measurements in (a) and (b) are performed on an a.p. sample with a slightly different sample geometry, which is described in [29].

by a pronounced reduction of J_{SC}, presumably due to improved charge-order and the resulting reduced carrier mobility. In the post-annealed junction, the vanishing of J_{SC} below 1.8 eV limits the photovoltaic effect, i.e. V_{OC} is below the resolution limit of our measurement setup. The spectrally resolved behavior of the CMO/STNO

Table 2. Temperature dependence of the open-circuit voltage under monochromatic illumination. Slope and intercept of the linear part at low temperatures (columns 2, 3) and activation barrier E_B of the Arrhenius-like part at high temperatures (column 4).

Heterojunction	dV_{OC}/dT (mV K^{-1})	$e{\cdot}V_{OC}(T \rightarrow 0)$ (meV)	E_B (meV)
PCMO/STNO (a.p.) $E_{ph} = 1.55$ eV	-2.60 ± 0.01	518 ± 2	508 ± 11
PCMO/STNO (p.a.) $E_{ph} = 1.55$ eV	-2.70 ± 0.14	494 ± 18	492 ± 29
CMO/STNO $E_{ph} = 2.0$ eV	-2.19 ± 0.01	310 ± 1	255 ± 15

junction is similar, i.e. V_{OC} and J_{SC} are almost constant above 2.6 eV, decrease simultaneously below 2.6 eV, and vanish at about 1.8 to 1.9 eV. These results clearly show that excitations in the manganites contribute to the photovoltaic effect.

5. Discussion

From the viewpoint of Shockley's theory, the J–V characteristic of a single diode p–n homojunction under illumination is given by [30, 31]:

$$J(V) = J_S \cdot \left(\exp\left[\frac{e \cdot V}{n \cdot k \cdot T} \right] - 1 \right) - J_{SC}, \tag{1}$$

where n is the ideality factor, k is the Boltzmann constant, J_S is the dark saturation current density of the junction, and J_{SC} the short-circuit current density. The open-circuit voltage V_{OC} is the potential required to balance the generation current by the thermally activated recombination current, and equation (1) implies

$$e \cdot V_{OC} = n \cdot k \cdot T \cdot \ln\left(\frac{J_{SC}}{J_S} + 1 \right). \tag{2}$$

Assuming that charge separation in the p–n heterojunctions is governed by a single dominant contribution to the thermally activated recombination current represented by an activation barrier E_B and a sufficiently large short-circuit current density $J_{SC} \gg J_S$, equation (2) can be rewritten as

$$e \cdot V_{OC} = E_B - n \cdot k \cdot T \cdot \ln\left(\frac{J_0}{J_{SC}} \right), \tag{3}$$

where J_0 is the temperature-independent prefactor of an Arrhenius-type temperature dependence of J_S, which depends on intrinsic material properties. In the case of homojunctions, E_B is determined by the band gap; meanwhile, in heterojunctions, E_B can be limited by the band offsets [29, 32]. V_{OC} should linearly scale with temperature and the logarithm of the short-circuit current density, and the relevant activation barrier can be deduced from the intercept $E_B = V_{OC}(T \rightarrow 0)$. Equation (3) is valid only if the diffusion length of the excess carriers is larger than the extension of the space charge region, thus reflecting a charge separation mechanism, where the photocurrent of minority charge carriers, i.e. the excess carrier diffusion from the bulk of the thin film absorber, is not the limiting factor.

Under polychromatic illumination, the linear temperature dependence of V_{OC} in the entire temperature range and the similar values of the slopes in PCMO/STNO and CMO/STNO junctions (figure 4(a)) point to a dominant contribution to the photovoltaic effect, which originates from excess carriers generated in the STNO. This is in accordance with recently published low-energy scanning transmission electron beam-induced current observations for PCMO/STNO junctions [33]. In addition, a strong increase of the short-circuit current due to STNO excitations was observed in [20]. The activation barrier E_B of PCMO/STNO junctions is increased for post-annealed samples from $E_B \approx 540$ meV to $E_B \approx 695$ meV. Post-growth annealing may affect $E_B$due to small cation intermixing at the interface [16] by charged defects like oxygen vacancies at the PCMO/STNO interface [19], or by a shift of the valence band in PCMO, e.g. change in Coulomb repulsion [23]. The latter may be induced by a vacancy-induced change of doping.

Under illumination conditions, where excitations in the STNO are excluded, the temperature dependence of V_{OC} of PCMO/STNO junctions reveals three regimes (see figure 6(c)). These regimes are also visible in the relation between V_{OC} and $\ln(J_{SC})$ (figure 8(a)), as deduced from the data in figure 5 (variation of the illumination spectrum at different temperatures):

(i) *The low-temperature regime,* which reveals non-linear relations between V_{OC} and $\ln(J_{SC})$ as well as $T < 140$ K, resembling a saturation behavior. In PCMO, charge mobility is controlled by thermally activated hopping processes of small polarons, which give rise to a high series resistance contribution at low temperatures. This seems to be the main origin of the strong decrease of the short-circuit current of

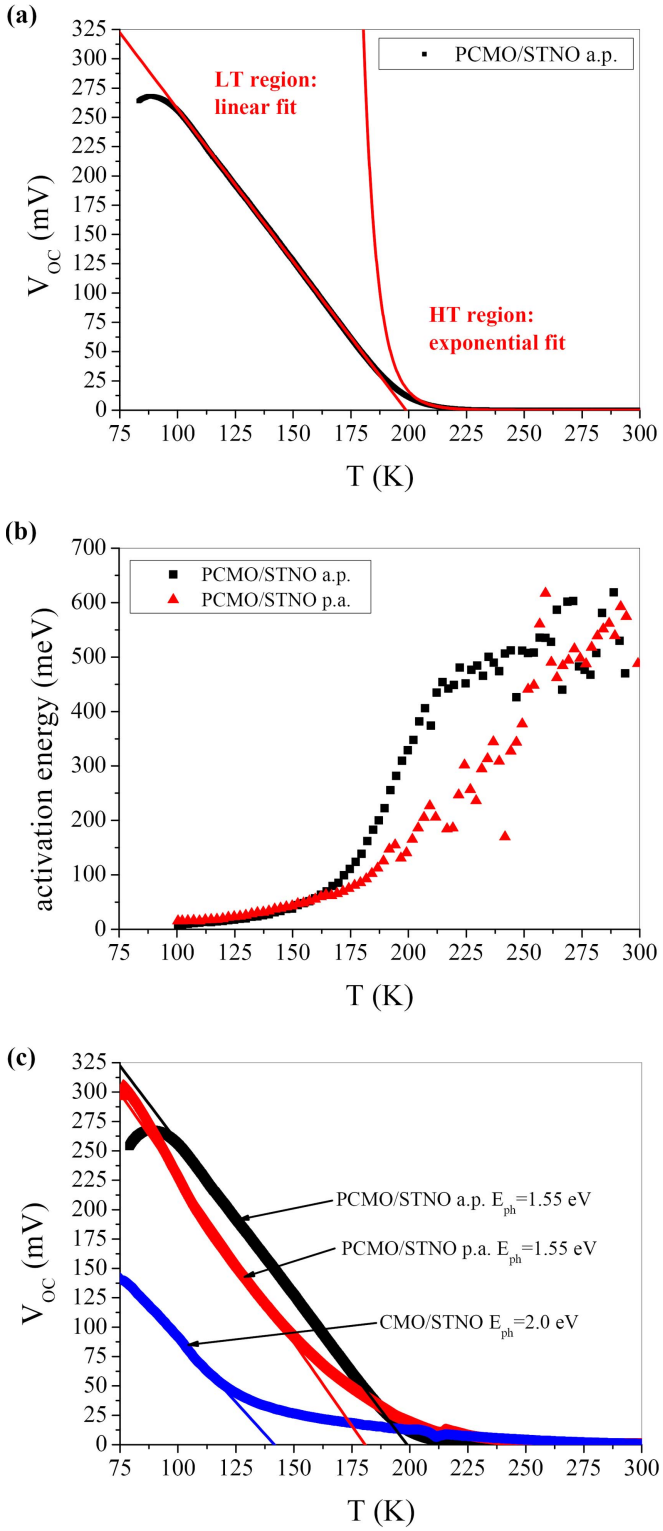

Figure 6. Temperature dependence of V_{OC} in manganite/titanite junction under monochromatic illumination. (a) $V_{OC}(T)$ measured at $E_{ph} = 1.55$ eV for an a.p. PCMO/STNO junction. A crossover from exponential to a linear temperature dependence is visible at $T = 200$ K. (b) Apparent activation energies for a.p. and post-annealed PCMO/STNO junctions derived from the logarithmic derivative of $V_{OC}(T)$. (c) Temperature dependence of the open-circuit voltage for the different junctions under monochromatic illumination. Lines are linear fits to the data.

PCMO/STNO junctions at temperatures below 200 K (figure 4(b)). Low mobility of localized charge carriers is also expected to cause saturation or reduction of V_{OC} at low temperatures, e.g. in organic solar cells [34].

(ii) *The medium-temperature regime*, where $T_{CO} > T > 140$ K. The photovoltaic effect is governed by excess carrier diffusion to the interface. The relation between V_{OC} and T as well as $\ln(J_{SC})$ is linear, which points to

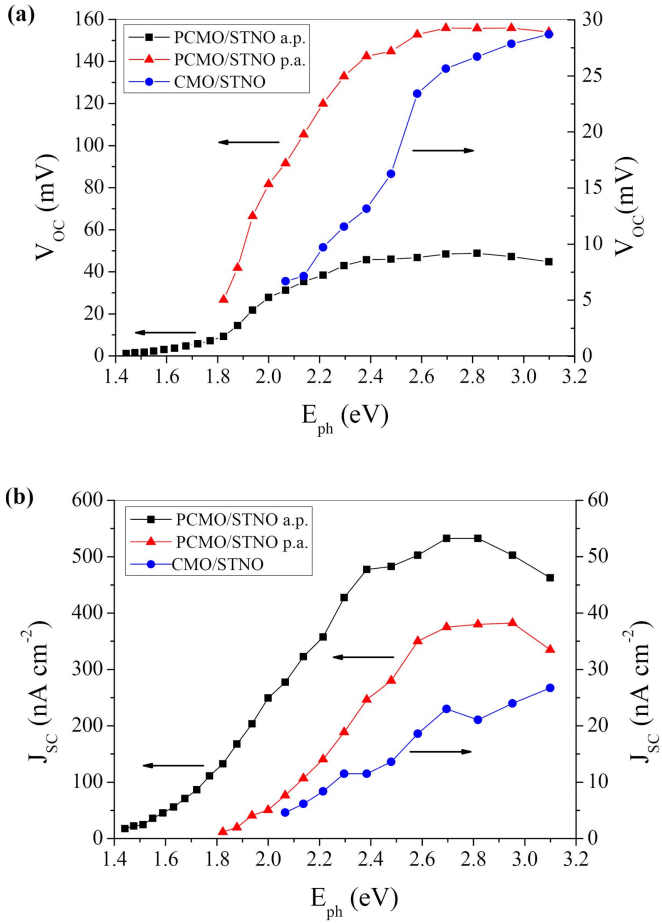

Figure 7. Spectrally resolved photovoltaic properties at T = 200 K for a.p. and post-annealed PCMO/STNO (squares and triangles) and CMO/STNO (circles) junctions. The low-energy end points essentially represent the vanishing of the photovoltaic effect due to the vanishing of J_{SC}, i.e. J_{SC} becomes smaller than the noise level of the device, which is about 10 nA cm^{-2}. (a) Open-circuit voltage V_{OC} versus photon energy E_{ph}. (b) Short-circuit current density versus photon energy E_{ph}. Left axis corresponds to PCMO/STNO, right axis to CMO/STNO. Lines are guides for the eyes.

a diffusion length of the excess carriers larger than the extension of the space charge region. This is in accordance with the assumptions for a Shockley-like model.

(iii) *The high-temperature regime*, where $T > T_{CO} \approx 200$ K revealing non-linear V_{OC}–ln(J_{SC}) characteristics with opposite curvature compared to the low-temperature regime: V_{OC} depends exponentially on T with an activation energy, which roughly equals the zero-temperature open-circuit voltage under monochromatic illumination.

In the high-temperature regime, the photocurrent from the PCMO to the STNO seems to be the limiting factor because the saturation current J_S is not much smaller than the short-circuit current J_{SC}. Assuming $J_S \gg J_{SC}$, equation (2) leads to an exponential temperature dependence of V_{OC}. For such low photocurrents, mainly photoexcitations at the interface might lead to the excess carrier generation, and thus the charge separation rate might be influenced by interfacial dipoles. We suggest that a $V_{OC} \propto \exp(E_B/kT)$ characteristic emerges, because the charge separation is governed by the competition between the photocurrent due to the photo-induced interface dipole forward transition and the thermally activated recombination current. An optical transition of the interface dipole is a dipole-allowed transition due to the different parity of the involved manganite e_g-O2p and titanite t_{2g} states. The activation energy in this scenario is still E_B.

The spectral dependence of the photovoltaic properties in figure 7 suggests that two photovoltaic relevant excitations in PCMO contribute to the V_{OC}, i.e. the JT transition from Mn3d e_g to O2p-e_g states and the CT transition between O2p states and t_{2g} states (figure 1). In figure 8(b) V_{OC} is plotted versus ln(J_{SC}) for the dataset of figure 7 (spectrally resolved measurements at $T = 200$ K). With increasing energy of the incident light, PCMO-STNO junctions reveal a crossover between two linear regimes with different slopes. According to equation (3), the two regimes correspond to two different transitions, i.e. the JT transition at lower energies and the CT transition at higher energies. CMO/STNO junctions mainly reveal a linear regime with a slope very

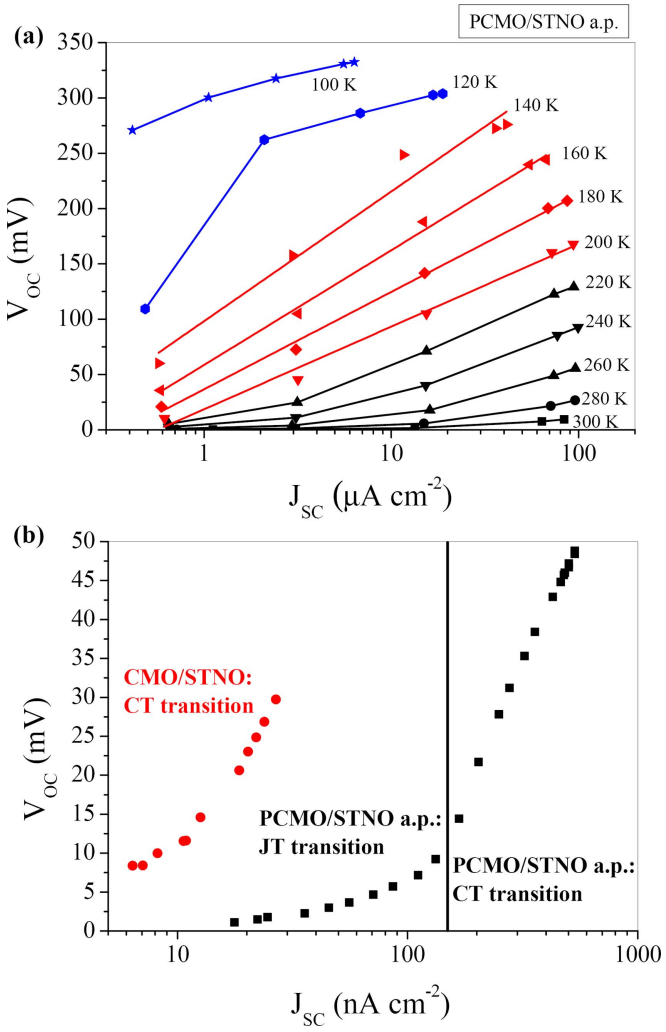

Figure 8. Open-circuit voltage V_{OC} versus ln(J_{SC}): (a) Analysis for the PCMO/STNO junction using the dataset from figures 5(a) and (b) for an a.p. PCMO/STNO junction: Cut-off filter for $E_{ph} < 1.6,1.9,2.8,3.5$ eV and xenon illumination, from left to right. The same symbols correspond to one temperature. The colors indicate the different regimes. Black symbols: Excess carrier generation at the interface. Red symbols: Excess carrier diffusion from volume. Blue symbols: Low mobility of polarons. Red lines represent linear fits to the data, whereas the blue and black lines are guides for the eyes. (b) Comparison of V_{OC} versus ln(J_{SC}) for PCMO/STNO (a.p.) and CMO/STNO junctions derived from the spectral measurement of V_{OC} and J_{SC} at $T = 200$ K in figure 7.

similar to the slope of the CT transition in PCMO. However, the short-circuit current densities in CMO/STNO junctions are much lower. In contrast to PCMO based junctions, the short-circuit current seems not to be limited by serial resistance contributions at low temperatures, resulting in a temperature-independent short-circuit current density (figure 4(b)). The reduction is most probably due to enhanced electron–hole recombination at APBs (see supplement section B).

The minimum excitation energy of about 1.3 eV, which gives rise to a photovoltaic effect in PCMO (figure 7), is larger than the band gap of PCMO in the CO phase ($E_{G,PCMO} = 0.37$ eV) [6]. Transitions between Mn3d e_g states are commonly dipole forbidden. Taking into account the hybridiziation of O2p states in a molecular orbital picture, the minimum excitation energies can be attributed to the dipole-allowed transition from non-bonding Mn3d e_g to antibonding σ type O2p-e_g states that set in at the absorption maximum of the polaron transition ferromagnetically coupled JT polarons at 1 .6 eV [35] (see also figure S1 supplement section A). In CMO, the JT splitting is absent and we therefore expect that the only photovoltaic relevant excitation in CMO is the CT transition between O2p states and e_g states, i.e. excitations above the CMO band gap (see supplement section A).

The most remarkable difference between transitions in the STNO and the manganites is the crossover to a Shockley-like bulk generation of photocarriers in the manganite in the medium-temperature regime. For PCMO/STNO junctions, the role of charge-ordering is evident in the temperature dependence of V_{OC} and J_{SC} (figures 5, 6(c)). Photoexcitations in PCMO give rise to an exponentially small open-circuit voltage at high temperatures and a linear increase at low temperatures. The key to explain this behavior is the recently observed long lifetime of polaronic excitations [34]. Combining optical pump–probe experiments and first principle

calculations, the authors conclude that cooperative behavior of polarons in highly doped manganites, e.g. the appearance of short- or long-range charge-order, is an essential prerequisite for long-living excited polaron states in PCMO. This is consistent with our analysis that below T_{CO}, excess carrier diffusion from outside the space charge region to the interface gives rise to the photovoltaic effect. Post-growth annealing facilitates the formation of the long-range charge-ordered phase, which in the framework of our model is reflected in an increase of V_{OC} (figure 7(a)). Indeed, in the charge-ordered state this seems to enable not only long lifetimes of photo-excited polarons in the JT transition (energies between 1.3 and 2 eV) but also for transitions into the minority spin t_{2g} states, which are populated above 2.4 eV as indicated by the increase of the photocurrent for $E_{ph} < 1.9$ to $E_{ph} < 2.8$ eV in figure 7(b). The charge transfer transition in CMO also gives rise to a crossover from exponential to linear temperature dependence of V_{OC} (figure 6), which takes place near the Neel temperature $T_N = 120$ K of anti-ferromagnetic ordering. This might indicate that lifetimes of charge transfer type excitations depend on the magnetic long-range order in CMO.

6. Summary

Spectrally resolved and temperature-dependent analysis of photovoltaic properties provide insights into the contribution of three optical transitions to photovoltaic energy conversion in manganite/titanite junctions. Under polychromatic illumination including optical excitations in the titanite, the photovoltaic effect is mainly governed by generation of excess carriers in the STNO. If the photocurrent is dominated by the generation of electron–hole pairs in STNO, the Shockley model is applicable in the entire temperature range. The similarity of PCMO/STNO and CMO/STNO junctions is mainly visible in the agreement of the slope of $V_{OC}(T)$, which reflects the density of states and lifetime of the STNO excitations.

In contrast, if the photocurrent is generated by photoexcitations in the manganites, a more sophisticated model of the underlying photovoltaic mechanisms is required. Here $V_{OC}(T \to 0)$ does not depend strongly on the involved manganite transitions, in contrast to the short-circuit current density J_{SC}. This indicates that the barrier for charge separation and photovoltage generation does not depend on the type of transition, and both the JT and CT transition contribute to the photovoltaic effect in PCMO/STNO junctions. Three different regimes are observed: (i) an interface-dominated transition above T_{CO}, (ii) a Shockley-like behavior below T_{CO}, and (iii) a freeze-in regime, where the small polaron mobility at $T < 140$ K limits charge separation. JT and CT transitions lead to distinguishable diode properties in a Shockley-type analysis of the V_{OC}–ln(J_{SC}) relation under monochromatic illumination.

The onset of a linear $V_{OC}(T)$ dependence below T_{CO} in PCMO and T_N in CMO suggests that sufficiently long lifetimes of photocarriers for diffusion from outside the space charge region to the interface are only present for long-range ordering of charge and spins in the manganites. However, the effect of charge-ordering on the photovoltaic performance is counteracting the ability to generate large photocurrents. In CMO/STNO junctions, due to the absence of CO, the photocurrents should be much higher but are most probably limited by the recombination at extended defects.

Acknowledgments

We thank Patrick Peretzki for valuable discussion. Funding from the Deutsche Forschungsgemeinschaft (DFG) under Grant No. SFB1073, project B02, is gratefully acknowledged.

References

[1] Dagotto E 2003 *Nanoscale Phase Separation and Colossal Magnetoresistance* 1st edn (Berlin: Springer)
[2] Tokura Y 2006 Critical features of colossal magnetoresistive manganites *Rep. Prog. Phys.* **69** 797
[3] Zhou J-S and Goodenough J B 2003 Orbital order-disorder transition in single-valent manganites *Phys. Rev.* B **68** 144406
[4] Goodenough J B 1955 Theory of the role of covalence in the perovskite-type manganites [La,M(II)]MnO_3 *Phys. Rev.* **100** 564
[5] Jirak Z 1985 Neutron diffraction study of $Pr_{1-x}Ca_xMnO_3$ perovskites *J. Magn. Magn. Mater.* **53** 153
[6] Mildner S, Hoffmann J, Blöchl P E, Techert S and Jooss C 2015 Temperature- and doping-dependent optical absorption in the small-polaron system $Pr_{1-x}Ca_xMnO_3$ *Phys. Rev.* B **92** 35145
[7] Moskvin A S, Makhnev A A, Nomerovannaya L V, Loshkareva N N and Balbashov A M 2010 Interplay of p-d and d-d charge transfer transitions in rare-earth perovskite manganites *Phys. Rev.* B **82** 35106
[8] Jung J H, Kim K H, Eom D J, Noh T W, Choi E J, Yu J, Kwon Y S and Chung Y 1997 Determination of electronic band structures of $CaMnO_3$ and $LaMnO_3$ using optical-conductivity analyses *Phys. Rev.* B **55** 15489
[9] Kaplan S G, Quijada M, Drew H D, Tanner D B, Xiong G C, Ramesh R, Kwon C and Venkatesan T 1996 Optical evidence for the dynamic Jahn-Teller effect in $Nd_{0.7}Sr_{0.3}MnO_3$ *Phys. Rev. Lett.* **77** 2081
[10] Ichikawa H *et al* 2011 Transient photoinduced 'hidden' phase in a manganite *Nat. Mater.* **10** 101
[11] Kiryukhin V, Casa D, Hill J P, Keimer B, Vigliante A, Tomioka Y and Tokura Y 1997 An x-ray-induced insulatormetal transition in a magnetoresistive manganite *Nature* **386** 813

[12] Sawa A, Fujii T, Kawasaki M and Tokura Y 2005 Highly rectifying $Pr_{0.7}Ca_{0.3}Mn0_3/SrTi_{0.9998}Nb_{0.0002}O_3$ p-n junction *Appl. Phys. Lett.* **86** 112508
[13] Sun J R, Zhang S Y, Shen B G and Wong H K 2005 Rectifying and photovoltaic properties of the heterojunction composed of $CaMnO_3$ and Nb-doped $SrTiO_3$ *Appl. Phys. Lett.* **86** 53503
[14] Lü W M, Sun J R, Wang D J, Xie Y W, Liang S, Chen Y Z and Shen B G 2008 Bias-dependent rectifying properties of n-n manganite heterojunctions $La_{1-x}Ca_xMnO_3/SrTiO_3$:Nb (x = 0.65-1) *Appl. Phys. Lett.* **93** 212502
[15] Muramatsu T, Muraoka Y and Hiroi Z 2004 Photocarrier injection and the I–V characteristics of $La_{0.8}Sr_{0.2}MnO_3/SrTiO_3$:Nb heterojunctions *Solid State Commun.* **132** 351
[16] Saucke G, Norpoth J, Jooss C, Su D and Zhu Y 2012 Polaron absorption for photovoltaic energy conversion in a manganite-titanate pn heterojunction *Phys. Rev.* B **85** 165315
[17] Schirmer O F, Imlau M, Merschjann C and Schoke B 2009 Electron small polarons and bipolarons in $LiNbO_3$ *J. Phys. Condens. Matter* **21** 123201
[18] Woike T, Berben D, Imlau M, Buse K, Pankrath R and Krätzig E 2001 Lifetime of small polarons in strontium-barium-niobate single crystals doped with cerium or chromium *J. Appl. Phys.* **89** 5663
[19] Norpoth J, Mildner S, Scherff M, Hoffmann J and Jooss C 2014 *In situ* TEM analysis of resistive switching in manganite based thin-film heterostructures *Nanoscale* **6** 9852
[20] Sheng Z G, Nakamura M, Koshibae W, Makino T, Tokura Y and Kawasaki M 2014 Magneto-tunable photocurrent in manganite-based heterojunctions *Nat. Commun.* **5** 4584
[21] Prokhorov V G, Kaminsky G G, Flis V S and Lee Y P 1999 Temperature dependence of resistance of $Pr_{0.65}Ca_{0.35}MnO_3$ films prepared by pulsed laser deposition *Low Temp. Phys.* **25** 792
[22] Souza J A, Neumeier J J, Bollinger R K, McGuire B, dos Santos C A M and Terashita H 2007 Magnetic susceptibility and electrical resistivity of $LaMnO_3$, $CaMnO_3$, and $La_{1-x}SrMnO_3$ ($0.13 \leqslant x \leqslant 0.45$) in the temperature range 300–900 K *Phys. Rev.* B **76** 24407
[23] Sotoudeh M, Rajpurohit S, Blöchl P, Mierwaldt D, Norpoth J, Roddatis V, Mildner S, Ifland B and Jooss C 2016 Electronic structure of $Pr_{1-x}Ca_xMnO_3$ (https://arxiv.org/abs/1610.07548)
[24] Jooss C, Wu L, Beetz T, Klie R F, Beleggia M, Schofield M A, Schramm S, Hoffmann J and Zhu Y 2007 Polaron melting and ordering as key mechanisms for colossal resistance effects in manganites *Proc. Natl. Acad. Sci. U. S. A.* **104** 13597–602
[25] Uehara M, Mori S, Chen C H and Cheong S-W 1999 Percolative phase separation underlies colossal magnetoresistance in mixed-valent manganites *Nature.* **399** 560
[26] Ahn K H, Lookman T and Bishop A R 2004 Strain-induced metal-insulator phase coexistence in perovskite manganites *Nature* **428** 401
[27] Hoffmann J, Moschkau P, Mildner S, Norpoth J, Jooss C, Wu L and Zhu Y 2014 Effects of interaction and disorder on polarons in colossal resistance manganite $Pr_{0.68}Ca_{0.32}MnO_3$ thin films *Mater. Res. Express* **1** 46403
[28] Gil De Muro I, Insausti M, Lezama L and Rojo T 2005 Morphological and magnetic study of $CaMnO_{3-x}$ oxides obtained from different routes *J. Solid State Chem.* **178** 928
[29] Ifland B, Peretzki P, Kressdorf B, Saring P, Kelling A, Seibt M and Jooss C 2015 Current–voltage characteristics of manganite-titanite perovskite junctions *Beilstein J. Nanotechnol.* **6** 1467
[30] Shockley W 1949 The theory of p-n junctions in semiconductors and p-n junction transistors *Bell Labs Tech. J.* **28** 435
[31] Shockley W and Queisser H J 1961 Detailed balance limit of efficiency of p-n junction solar cells *J. Appl. Phys.* **32** 510
[32] Teran A S, Member S, Chen C, Linares P G, Artacho I and Mart A 2015 Heterojunction band offset limitations on open-circuit voltage in p-ZnTe/n-ZnSe solar cells *IEEE J. Photvoltaics* **5** 874
[33] Peretzki P, Ifland B, Jooss C and Seibt M 2017 Low energy scanning transmission electron beam induced current for nanoscale characterization of p–n junctions *Phys. Status Solidi RRL* **11** 1600358
[34] Qi B, Zhou Q and Wang J 2015 Exploring the open-circuit voltage of organic solar cells under low temperature *Sci. Rep.* **5** 11363
[35] Raiser D, Mildner S, Ifland B, Sotoudeh M, Blöchl P, Techert S and Jooss C 2017 Evolution of hot polaron states with a nanosecond lifetime in a manganite perovskite *Adv. Energy Mater.* **2017** 1602174